

Ultrafast Solvation Dynamics of Human Serum Albumin: Correlations with Conformational Transitions and Site-Selected Recognition

Weihong Qiu,[†] Luyuan Zhang,[†] Oghaghare Okobiah, Yi Yang, Lijuan Wang, and Dongping Zhong*

Departments of Physics, Chemistry, and Biochemistry, Programs of Biophysics, Chemical Physics, and Biochemistry, 191 West Woodruff Avenue, The Ohio State University, Columbus, Ohio 43210

Ahmed H. Zewail*

Laboratory for Molecular Sciences, Noyes Laboratory of Chemical Physics, California Institute of Technology, Pasadena, California 91125

Received: October 19, 2005; In Final Form: January 17, 2006

Human serum albumin, the most abundant protein found in blood plasma, transports a great variety of ligands in the circulatory system and undergoes reversible conformational transitions over a wide range of pH values. We report here our systematic studies of solvation dynamics and local rigidity in these conformations using a single intrinsic tryptophan (W214) residue as a local molecular probe. With femtosecond resolution, we observed a robust bimodal distribution of time scales for all conformational isomers. The initial solvation occurs in several picoseconds, representing the local librational/rotational motions, followed by the dynamics, in the tens to hundreds of picoseconds, which result from the more bonded water in the tryptophan crevice. Under the physiological condition of neutral pH, we measured ~ 100 ps for the decay of the solvation correlation function and observed a large wobbling motion at the binding site that is deeply buried in a crevice, revealing the softness of the binding pocket and the large plasticity of the native structure. At acidic pH, the albumin molecule transforms to an extended conformation with a large charge distribution at the surface, and a similar temporal behavior was observed. However, at the basic pH, the protein opens the crevice and tightens its globular structure, and we observed significantly faster dynamics, 25–45 ps. These changes in the solvation dynamics are correlated with the conformational transitions and related to their structural integrity.

I. Introduction

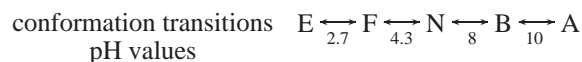
Biomolecular recognition is mediated by water motions, and the dynamics of associated water directly determines local structural fluctuation of interacting partners.^{1–3} The time scales of these interactions reflect their flexibility and adaptability. For water at protein surfaces, our recent studies^{4–6} of hydration dynamics (tens of picoseconds) suggest that these mobile surface water layer molecules are constantly in exchange with outside bulk water. For trapped water in protein crevices or cavities, the dynamics becomes much slower and could extend to nanoseconds.^{7–9} These rigid water molecules are often hydrogen-bonded to interior residues and become part of the structural integrity of many enzymes.⁷

Earlier we studied protein hydration with tryptophan being at the surface.^{5,6} The purpose of this work is to study local water motions in various environments, from a buried crevice to an exposed surface, using site-selected tryptophan but with different protein conformations. The aim is to understand the correlation between hydration dynamics and conformational transitions and then relate them to biological function.

The structure and hydration of human serum albumin (HSA) are important for the transport of fatty acids and for binding a great variety of metabolites, drugs, and organic compounds in the circulatory system.^{10,11} It is a single polypeptide chain

consisting of 585 amino acids. Under physiological conditions (pH ≈ 7), HSA adopts a heart-shaped three-dimensional structure with three homologous domains I–III (Figure 1); each domain contains two subdomains A and B that consist of 4 and 6 α -helices, respectively.^{12,13} The X-ray structure shows that two halves of the albumin molecule form a 10-Å-wide, 12-Å-deep crevice that is filled with water molecules.^{12,13} The only single tryptophan residue W214 in the protein is located in the binding site IIA at the bottom of the crevice (Figure 1).

With the change in pH, HSA undergoes reversible conformational isomerization, and pH-dependent isomers were first demonstrated by Luetscher¹⁴ in 1939 and later systematically classified by Forster¹⁵ in 1960. At neutral pH, the conformation of HSA is in its common physiological state, referred as a norm form (N); an abrupt transition occurs at a pH value of less than 4.3, changing the N form to the so-called fast migrating form (F), and when the pH is less than 2.7, a further transition takes place from the F form to the extended form (E). On the other side of the scale, when the pH value becomes above 8, the N conformation changes to the basic form (B), and at a pH above 10 the structure transforms to another aged form (A). These transitions are summarized below.¹⁰



The protein has been extensively studied in every aspect due to its physiological importance and its potential as a drug delivery vehicle^{10,11} and because different acidic and basic

* Authors to whom correspondence should be addressed. E-mail: dongping@mps.ohio-state.edu; zewail@caltech.edu.

[†] These authors contributed equally to this work.

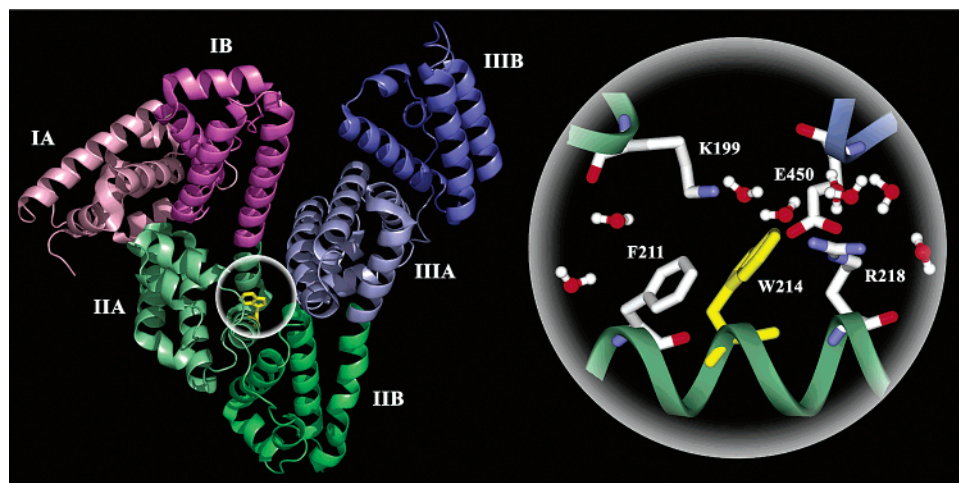


Figure 1. Left panel: X-ray crystallographic structure of human serum albumin¹³ at the neutral pH condition. The three constituting domains I, II, and III are in purple, green, and blue, respectively. Note a deep crevice between the two halves of the structure with W214 (in yellow) located at the bottom. Right panel: Local configuration around W214 with eight trapped water molecules within 7 Å and four potential tryptophan fluorescence quenching residues in close proximity of less than 5 Å.

isomers may have certain biological functions.^{16,17} Most studies have focused on binding interactions with various ligands and revealed that HSA is an assembly of squirming and resilient components that frequently change in conformation through opening and closing of major crevices. With this “breathing” motion, HSA assimilates and releases a variety of substances during transportation in the circulatory system. Many complex structures have also been resolved at high X-ray resolution.^{12,18,19} The flexibility to adopt different conformations with independent segmental movements has also been shown through certain independent and sequential folding/unfolding studies of individual subdomains.^{20,21} The tryptophan W214 and extrinsic labeled dye molecules have been used as optical probes to study the conformational dynamics through changes in fluorescence lifetime, resonance energy transfer, and time-resolved anisotropy.^{22–26} The significant change in the lifetime of W214 for a series involving mutation in the binding site IIA clearly showed the local flexibility.²⁷

Previously, we reported studies of binding interactions²⁸ and hydration dynamics of protein unfolding,²¹ elucidating the rigid hydrophobic recognition and the different water mobility in three domains. In this study, we conducted a systematic investigation of the femtosecond-resolved fluorescence dynamics of tryptophan (W214) in HSA with the aim to understand the dynamics and structural flexibility under physiological conditions (N form) and to reveal the dynamical changes for conformational transitions occurring at different pH values. Because it is known that water is present (eight water molecules shown in Figure 1) around tryptophan in the crevice of the N conformation the dynamics should reflect the influence of their motions. The paper is organized as follows. Section II describes the experimental methodology including the femtosecond up-conversion laser setup and sample preparation. In section III, we present the femtosecond-resolved experimental results, and the discussion is given in section IV, focusing on the correlation of our results with conformational flexibility and transition. Finally, we conclude the work in section V.

II. Experimental Section

A. Femtosecond Up-Conversion Laser Setup. All of the femtosecond-resolved measurements were carried out using the femtosecond-resolved fluorescence up-conversion apparatus described elsewhere.²⁹ Briefly, the femtosecond pulse after the

two-stage amplifier (Spitfire, Spectra-Physics) has a temporal width of 110 fs centered at 800 nm with a pulse energy of more than 2 mJ and a repetition rate of 1 kHz. Half of the laser energy was used to pump an optical parametric amplifier (OPA-800C, Spectra-Physics) to generate signal (1242 nm) and idler (2248 nm) beams. The latter was mixed with the residual fundamental beam (800 nm) in a 0.2-mm-thick barium borate crystal (BBO, type I) to generate a femtosecond pulse centered at 590 nm. This laser pulse, which was compressed through a pair of prisms with double paths to produce a temporal resolution of 60 fs, was frequency-doubled to generate the pump wavelength at 295 nm using another 0.2-mm-thick BBO crystal. The 295-nm excitation wavelength was chosen to minimize tyrosine residue absorption and dominantly excite the single W214 residue;³⁰ the observed fluorescence essentially results from the excited W214 emission. The pump pulse energy was typically attenuated to ~140 nJ prior to being focused into the motor-controlled rotating sample cell.

The fluorescence emission was collected by a pair of parabolic mirrors and mixed with a gating pulse from another half of the fundamental beam (attenuated) in a 0.2-mm BBO crystal through a noncollinear configuration. The up-converted signal ranging from 218 to 292 nm was detected by a photomultiplier coupled with a double-grating monochromator. The instrument response time under the current noncollinear geometry is between 350 and 450 fs as determined from the up-conversion signal of Raman scattering of water around 326 nm. The pump beam polarization was set at the magic angle (54.7°) with respect to the acceptance axis (vertical) of the up-conversion crystal, and the polarization of the gating beam was set parallel to this axis through a half-wave plate. For fluorescence anisotropy measurements, the pump beam polarization was rotated to either parallel or perpendicular to the acceptance axis to obtain the parallel (I_{\parallel}) and perpendicular (I_{\perp}) signal, respectively. These transients were used to construct the time-resolved anisotropy: $r(t) = (I_{\parallel} - I_{\perp}) / (I_{\parallel} + 2I_{\perp})$.

B. Materials and Sample Preparation. HSA (essentially free of fatty acids and globulin) was obtained from Sigma-Aldrich in lyophilized powder and used without further purification. All of the other chemical reagents were purchased from Fisher Scientific. Protein stock solutions of 0.5 mM HSA were prepared by dissolving the lyophilized powder in corresponding buffers to make various isomers (N form, 10 mM sodium

phosphate, pH 7.0; F form, 10 mM sodium acetate, pH 4.1; E form, 10 mM sodium acetate/HCl, pH 2; B form, 10 mM Borax, pH 9.0; and A form, 10 mM Na₂HPO₄/NaOH, pH 11.0). For all femtosecond-resolved measurements, protein solutions were used without further dilution while sample solutions were diluted to ~10 μ M for the measurement of steady-state fluorescence spectra. Protein stock solution at pH 11.0 was incubated at 4 °C for more than 24 h before any spectroscopic measurements.

C. Steady-State Fluorescence Characterization. The steady-state fluorescence spectra were taken using a SPEX Fluoro-Max-3 spectrometer. All of the protein samples were excited at 295 nm to ensure the dominant fluorescence emission from the single W214. At neutral pH, the emission spectrum of HSA has an intensity maximum at 338 nm, similar to the surface tryptophan emission,^{5,6} indicating a highly polar environment with a large amount of trapped water around W214 in the crevice, as also confirmed by the crystallographic structure¹³ (Figure 1). The emission peak is shifted to the blue at 332.6 nm when pH is reduced to 4.1, suggesting a less polar microenvironment surrounding W214 when the protein undergoes N \rightarrow F conformational transition. At pH 2.0, though the protein structure expands to its maximum extent allowed by the internal disulfide linkages, the rearrangement of subdomain structures leads to a further blue shift of the emission maximum to 330 nm, indicating a more hydrophobic environment around W214 in conformational transition from F to E. In the slightly alkaline pH region (pH 9.0), HSA exhibits an emission spectrum with a peak at 336 nm, indicating a slight change of local polarity around W214 upon N \rightarrow B transition. At pH 11.0, no significant further shift of emission maximum was observed for the A form while the spectrum width becomes slightly narrower compared with the emission from the B form, suggesting similar local polarity.

D. Construction of the Solvation Correlation Function. The solvation correlation function was constructed following the method developed by Zhong and co-workers.³¹ In brief, all femtosecond-resolved fluorescence up-conversion transients are described by a sum of two terms of discrete exponential functions

$$I_{\lambda}(t) = I_{\lambda}^{\text{solv}}(t) + I_{\lambda}^{\text{popul}}(t) = \sum_i \alpha_i e^{-t/\tau_i} + \sum_j \beta_j e^{-t/\tau_j} \quad (\text{II.1})$$

where the first term, with parameters α_i and τ_i , represents solvation contribution while the second term, with parameters β_j and τ_j , represents the intrinsic lifetime (population) decay. The *overall* time-resolved emission spectra are constructed as follows

$$I(\lambda, t) = \frac{I_{\lambda}^{\text{ss}} I_{\lambda}(t)}{\sum_i \alpha_i \tau_i + \sum_j \beta_j \tau_j} \quad (\text{II.2})$$

where the I_{λ}^{ss} denotes the steady-state emission intensity at wavelength λ . In a similar manner, the lifetime-associated time-dependent emission spectrum is constructed according to

$$I^{\text{popul}}(\lambda, t) = \frac{I_{\lambda}^{\text{ss}} I_{\lambda}^{\text{popul}}(t)}{\sum_i \alpha_i \tau_i + \sum_j \beta_j \tau_j} \quad (\text{II.3})$$

The resulting time-resolved emission spectra, a function of fluorescence intensity versus frequency in cm^{-1} , are further fitted

with a log-normal function to deduce the *overall* emission maximum $\nu_s(t)$ and the lifetime-associated emission maximum $\nu_l(t)$.

Typically, the solvation time (τ_i) is shorter than the lifetime (τ_j). The complete solvation time is defined as τ_{sc} when the difference between $\nu_s(t)$ and $\nu_l(t)$ reaches 0.5 cm^{-1} . The corresponding emission peak is denoted as ν_{sc} . Apparently, these two emission maxima would no longer differentiate themselves after the solvation contribution diminishes. It is also readily realized that the probe tryptophan has not yet reached its steady-state emission peak ν_{ss} and the corresponding time (τ_{ss}), when the femtosecond-resolved spectrum reaches its steady-state emission maximum, is longer than the complete solvation time τ_{sc} . After solvation is completed, the femtosecond-resolved emission spectra continue to move to the red side due to the existence of multiple lifetimes with distinct emission peaks. Thus, the solvation response function is constructed by subtracting the lifetime-associated emission contribution $\nu_l(t)$ from the *overall* femtosecond-resolved emission maximum $\nu_s(t)$ as follows

$$c(t) = \frac{\nu_s(t) - \nu_l(t)}{\nu_s(0) - \nu_l(0)} \quad (\text{II.4})$$

The derived $c(t)$ function is fitted with a multiple-exponential decay function.

III. Results

A. Femtosecond-Resolved Fluorescence Dynamics. A series of femtosecond-resolved fluorescence up-conversion transients of HSA for different isomers are shown in Figures 2–6. More than eight transients of emission wavelengths, spanning from the blue to the red side, were collected for each isomer configuration. For each conformation, all fluorescence transients were analyzed with a global fitting strategy. Typically, four discrete exponential functions were used, two of which are the lifetime emission decays. The two fluorescence lifetimes varied depending on pH value but were fixed for all transients of a given isomer.

The lifetimes were determined carefully because they would affect the time scale of slow solvation dynamics. A series of transients at the red side of wavelengths, from 360 to 380 nm, was obtained, and the two lifetimes, with different ratios, are well fitted for these red-side transients. The longer lifetime is determined by conventional photon-counting measurement (from the literature), and the shorter one was obtained by fitting our 3-ns-long transients. Finally, these two lifetimes were used to fit all other transients, and all parameters from the fits are self-consistent (Supporting Information).

The longer lifetime of the N form is 6.1 ns,²² and the shorter one from our 3-ns transients was determined to be 1.4 ns. The red-side transients of the F form are nearly the same as those from the N form; thus the F form has the same two lifetimes. By comparison of red-side transients of other isomers, we determined the lifetimes of 912 ps and 4.6 ns for the E form, 1.15 and 6.1 ns for the B form, and 318 ps and 3.8 ns for the A form. However, it should be pointed out that because the time interval between two consecutive pump excitations is 2 ms and each transient was averaged over more than 1 h, for each isomer all fluctuated configurations would probably be sampled on such long times. Thus, the apparent two lifetimes do not mean that only two static configurations are present, but they mainly represent two types of temporal configuration distributions; the system is in dynamic heterogeneity.

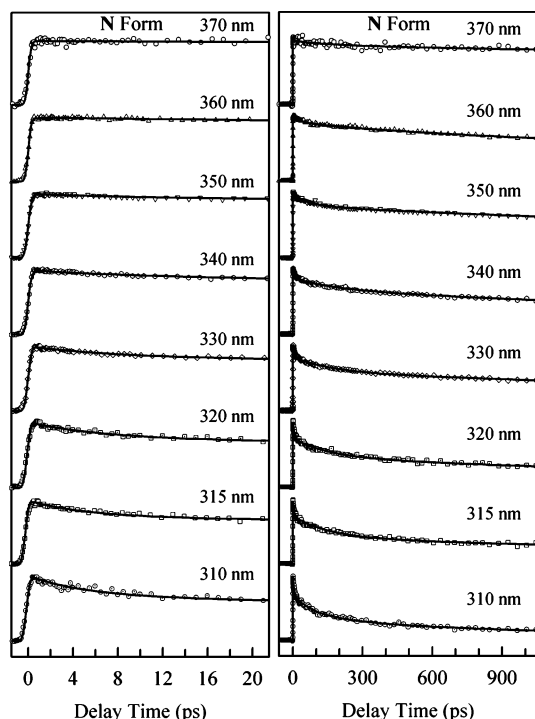


Figure 2. Normalized, femtosecond-resolved fluorescence transients of the N isomer in the short (left) and long (right) time ranges, with a series of gated fluorescence emissions. Note that solvation dynamics is significantly slower than that of tryptophan in a similar buffer.³¹

1. *N Form.* Figure 2 shows the femtosecond-resolved fluorescence transients of W214 for several typical wavelengths. The overall decay dynamics is significantly slower than that of aqueous tryptophan in a similar buffer solution.³¹ Clearly, the ultrafast decay components (<1 ps) observed in tryptophan solution were not observed at the blue side for the protein. The two exponential decays of solvation have time constants of 4.4–9.2 ps and 104–125 ps for all the blue-side transients. At the red side, we also observed a decay component of 51 ps with $\sim 10\%$ of the total amplitude, which results from the excited-state quenching of W214 by the neighboring residue(s), as discussed below.

2. *F Form.* Figure 3 shows the representative femtosecond-resolved fluorescence transients in the F conformation at pH 4.1. At the blue side, the solvation dynamics are represented by two decay components of 4.1–10.7 ps and 125–208 ps, respectively. Similarly, we did not observe ultrafast components (<1 ps) at the blue side. The second solvation component slows down, and its percentage increases after the $N \rightarrow F$ transition. We also observed a quenching component of 100 ps with an amplitude of about 10% in all the red-side transients.

3. *E Form.* The femtosecond-resolved transients of the E form at pH 2 are shown in Figure 4. At the blue side, the first solvation component slows down, and the dynamics occurs in 6.7–16.2 ps. The second component becomes relatively shorter (72–120 ps) from the $F \rightarrow E$ transition. These changes certainly reflect different local environments. The quenching contribution at the red side is reduced, and a decay component of 46 ps with $\sim 5\%$ amplitude was observed.

4. *B Form.* Figure 5 presents a set of selected femtosecond-resolved fluorescence transients from the B form at pH 9.0. At the blue side, two solvation components were observed in 1.1–3.1 ps and 32–45 ps, respectively. This observation is striking, and the solvation dynamics is drastically different from those observed in the N, F, and E isomers. Both solvation time scales

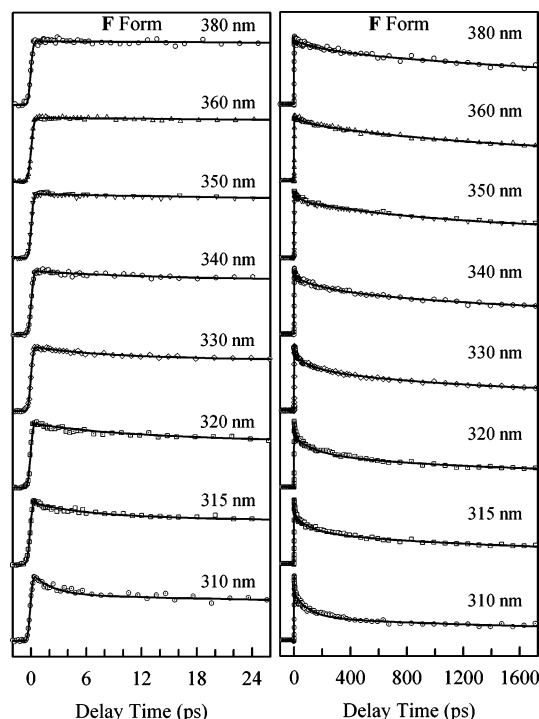


Figure 3. Normalized, femtosecond-resolved fluorescence transients of the F conformation in short (left) and long (right) time ranges, with a series of gated fluorescence emissions.

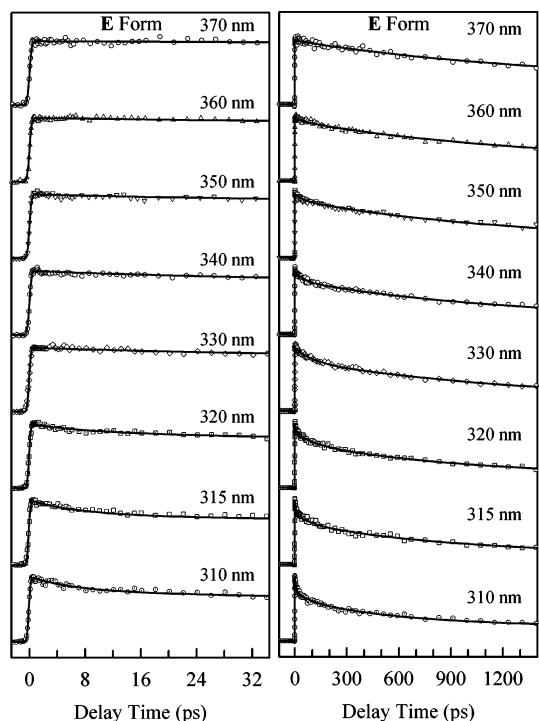


Figure 4. Normalized, femtosecond-resolved fluorescence transients of the E form in short (left) and long (right) time ranges, with a series of gated fluorescence emissions.

are significantly faster, indicating a large conformational change. At the red side, we observed a faster quenching component of 35 ps with an increasing amplitude of 10–20%.

5. *A Form.* Figure 6 shows representative femtosecond-resolved fluorescence transients in the A form under the extreme pH value of 11.0. Under such conditions, the conformation significantly changes, and at the red side, a considerable quenching component with a time constant of 29 ps and an amplitude of

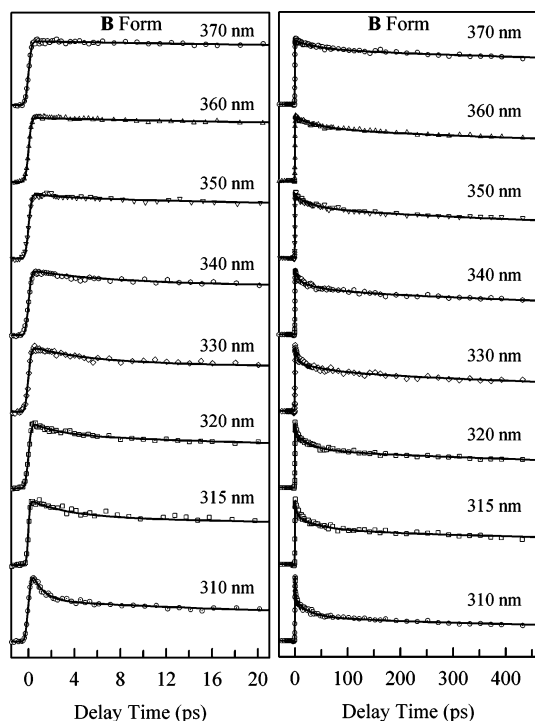


Figure 5. Normalized, femtosecond-resolved fluorescence transients of the B isomer in short (left) and long (right) time ranges, with a series of gated fluorescence emissions. Note that solvation dynamics becomes much faster than those reported in Figures 2–4 and also the quenching component at the red side becomes faster.

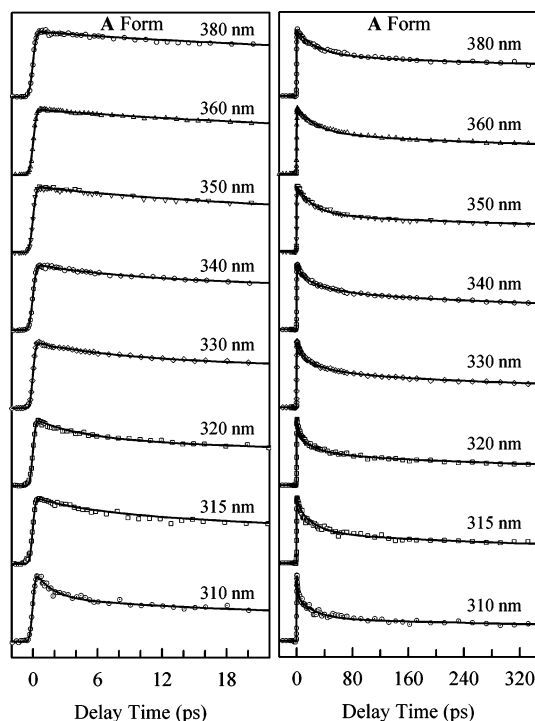


Figure 6. Normalized, femtosecond-resolved fluorescence transients of the A conformation in short (left) and long (right) time ranges, with a series of gated fluorescence emissions. Note the large, fast quenching component at the red side of the fluorescence emission.

37% was observed. At the blue side, solvation dynamics occurs in 1.1–3.5 ps and 15–28 ps, similar to the time scales observed in the B form, but with different amplitude percentages.

B. Solvation Correlation Function. Following eqs II.2 and II.3, we constructed the *overall* and *lifetime-associated* femtosecond-resolved emission spectra (FRES) for all conformational

isomers (Supporting Information). Figure 7 shows overall femtosecond-resolved emission maxima ν_s and lifetime-associated emission maxima ν_l , retrieved by fitting FRES to a log-normal function. Table 1 summarizes derived various emission maxima and times of different conformational isomers. Clearly, the complete solvation time τ_{sc} and the corresponding overall emission maximum ν_{sc} are quite different from τ_{ss} and ν_{ss} , respectively. The solvation correlation functions were constructed according to eq II.4, and the derived results are shown in Figure 8 and summarized in Table 2.

We carefully considered the contribution of vibration relaxation to the obtained total Stokes shifts by examining the change of FRES bandwidth with time. We observed an initial bandwidth broadening, *not narrowing*, of FRES, and such an increase in bandwidth is probably due to the initial wave packet dynamics. Thus, no noticeable contributions of vibration relaxation were observed, consistent with a 295-nm excitation at the red edge of tryptophan absorption. We also estimated whether the residual quenching in the red-side transients affects the overall solvation correlation function and constructed the *overall* and *lifetime-associated* FRES for all conformational isomers without taking into account the quenching contribution in all the red-side transients. No appreciable differences in the correlation function were observed except for the A form isomer. For simplicity, we constructed the correlation function for the A conformation by including all the quenching contributions.

As shown in Figure 8, conformational isomers exhibit very different solvation dynamics around W214. In the N form, the solvation correlation function is best represented by two exponential decays with the time constants of 5.0 ps with a 39% of the total amplitude and 133 ps (61%). The solvation times in the F form change to 4.3 ps (30%) and 186 ps (70%), respectively. The second long solvation dynamics slows down by about 40%. In the extended E form, the obtained solvation dynamics occurs in 6.7 ps (39%) and 108 ps (61%); the former is the longest time scale in the initial solvation, and the latter is the shortest in the second relaxation among these three (N, F, and E) conformers. For the B form isomer, the solvation dynamics has two time constants of 1.6 ps (30%) and 46 ps (70%), faster than those in the N form by a factor of 3. For the aged form A, the solvation correlation function has two exponential decay components of 2.3 ps (76%) and 27 ps (24%); the percentages are different from those obtained for the B form, and the overall solvation dynamics becomes much faster.

C. Femtosecond-Resolved Anisotropy Dynamics. We also studied the femtosecond-resolved rotational dynamics by the measurement of anisotropy changes with time. Figure 9 shows the anisotropy dynamics for the different isomers. All results are well fitted by three exponential decays, and the total anisotropy is well expressed by a sum of three parts: $r(t) = r_l + r_w + r_T$. The initial ultrafast decay (r_l) is in about 100 fs, which results from internal conversion between the two electronically excited states of 1L_a and 1L_b , as observed before.^{4,32} The anisotropy for all transients initially drops to a value of ~ 0.15 in such a short time, and this *apparent* anisotropy ($r_{app} \approx 0.15$) is consistent with the early reported value at excitation of 295 nm.³³ The second component (r_w) represents the local wobbling motion of W214, which reveals the local packing and backbone rigidity. The wobbling semiangle (θ) was estimated using the model of an axially symmetric oscillation about a fixed axis,³⁴ giving the expression

$$1 - \frac{r_w}{r_{app}} = \left[\frac{3 \cos^2 \theta - 1}{2} \right]^2 \quad (\text{III.1})$$

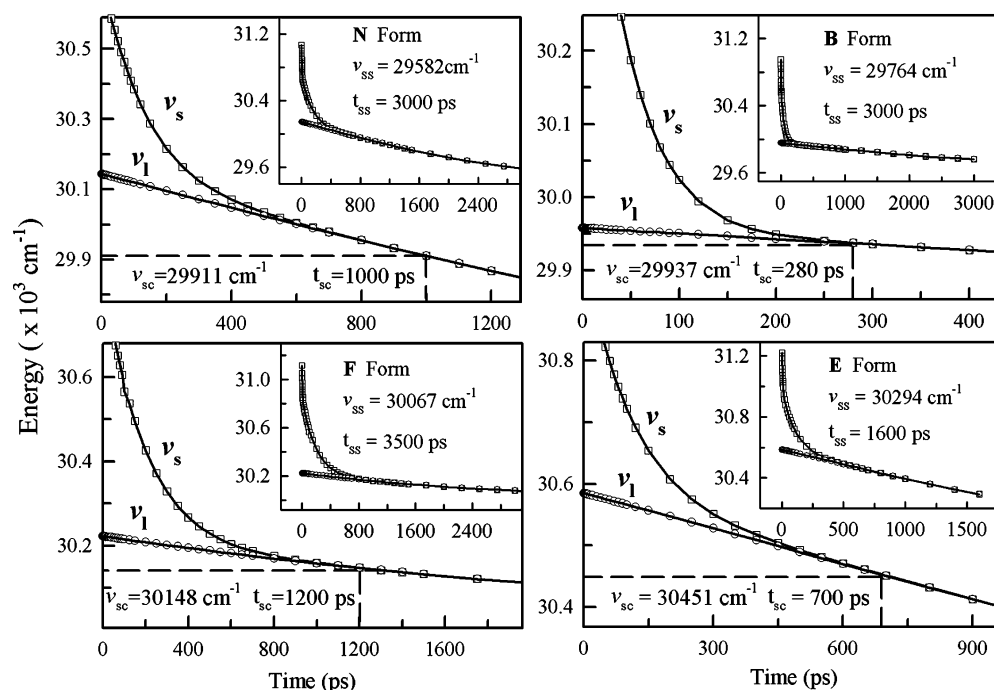


Figure 7. Femtosecond-resolved emission maxima of the overall emission spectra (ν_s) and the lifetime-associated emission spectra (ν_l) for four typical conformational isomers. The insert shows the entire evolution of ν_s and ν_l to reach the steady-state emission (ν_{ss}).

TABLE 1: Emission Maxima and Time Constants of W214 from Constructed Time-Resolved Spectra^a

isomer	λ_0	λ_{sc}	τ_{sc}	λ_{ss}	τ_{ss}	λ_1	λ_2
N	321.88	334.33	1000	338.0	3000	326.90	340.49
F	321.36	331.70	1200	332.6	3500	326.83	333.03
E	320.30	328.40	700	330.0	1600	323.61	332.53
B	323.08	334.03	280	336.0	3000	327.02	336.71
A ^b	327.43	334.05	150	336.0	1500	330.01	336.32

^a All emission maxima ($\lambda = 1/\nu$) and time constants (τ) are in units of nanometers and picoseconds, respectively. ^b The construction of the emission spectrum at time zero (λ_0) includes the quenching component.

The resulting semiangles are given in Figure 9. It is striking that the normal form (N) has the largest value of r_W and thus has the biggest wobbling semiangle of 24° , about double those of semiangles derived in E, F, and B conformational isomers. The last term r_T is the global tumbling motion of the entire protein, and the time scale was estimated to be about $\sim 22 \text{ ns}$.²⁵

IV. Discussion

A. Two Distinct Time Scales and Two Types of Dynamic Motions. For all conformational isomers, we observed two distinct time scales for solvation dynamics, and these results are robust, as we also observed in other systems.^{5,6,31} The constructed solvation correlation function is the response of the local environment around tryptophan to the sudden charge rearrangement from the ground state to the excited state. In principle, the response mainly results from both surrounding water molecules and neighboring protein polar/charged residues. Usually the motions of water molecules and their associated protein residues cannot be completely decoupled. However, the motion of protein residues highly depends on the local protein packing and structural rigidity. On the other hand, water molecules are much more mobile and easy to proceed to various motions under energy fluctuation. For tryptophan residues located at protein surfaces, we have revealed that the obtained correlation function is dominant from the local water cluster/network response.^{5,6} For tryptophan partially exposed to protein surfaces or buried inside proteins, the response function could

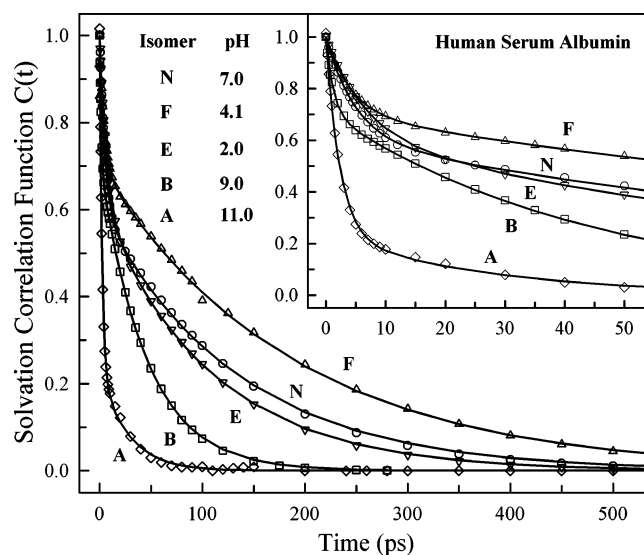


Figure 8. Solvation correlation functions probed by tryptophan (W214) in the five conformational isomers studied. The insert shows the correlation function in the short-time range. Note the large difference upon changing from the acidic to basic condition. The solvation correlation function of the A form was constructed by including the quenching contribution; see text.

be from a combined contribution of water molecules and protein residues, depending on the local protein rigidity. However, it is not conceivable that the response function is *only* from protein residues, not water at all, because water always accompanies residue fluctuations, especially at protein surfaces. We did not observe any ultrafast component ($< 1 \text{ ps}$), for all isomers, contrary to recent molecular dynamics (MD) simulations.^{35–37} Given that we were able to resolve the 200 fs of tryptophan solvation in bulk water,^{4–6,31} this lack of observation of sub-picosecond solvation suggests that the force field used in the MD simulations might be too flexible.

The observed initial solvation dynamics, occurring in several picoseconds, represents the local librational/rotational motions

TABLE 2: Results Obtained from Solvation Correlation Functions $c(t)$ of Different Isomers^a

isomer	τ_1	τ_2	c_1	c_2
N	5.0	133	0.39	0.61
F	4.3	186	0.30	0.70
E	6.7	108	0.39	0.61
B	1.6	46	0.30	0.70
A ^b	2.3	27	0.76	0.24

^a Solvation correlation functions were best fitted with $c(t) = c_1 e^{-t/\tau_1} + c_2 e^{-t/\tau_2}$, where $c_1 + c_2 = 1$. The time constants are in units of picoseconds. ^b The time scales were obtained by a construction of the correlation function, including the quenching component.

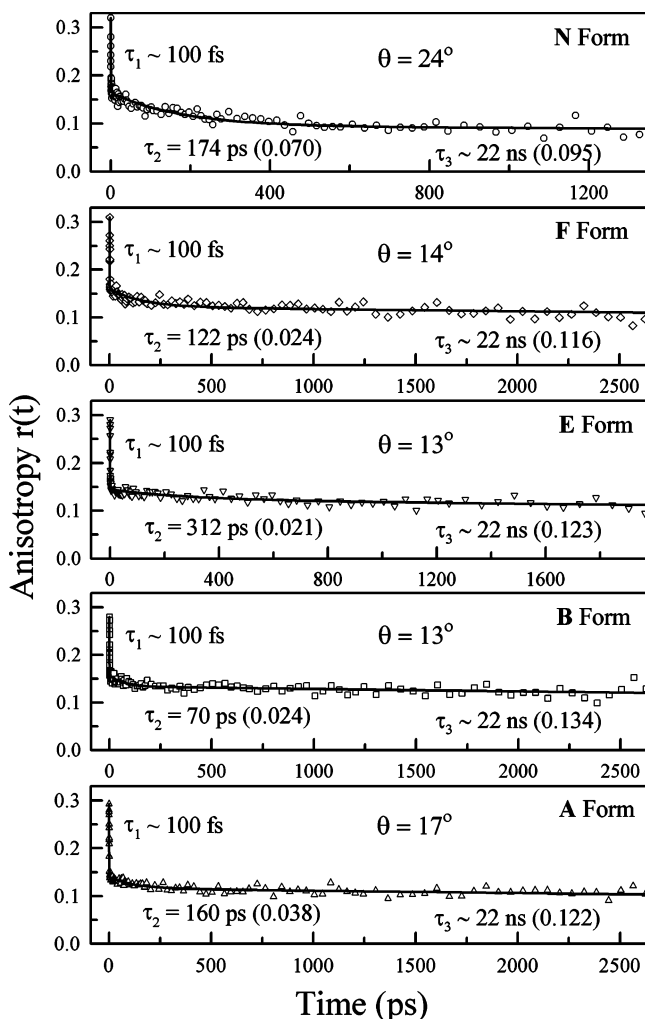


Figure 9. Femtosecond-resolved fluorescence anisotropy of W214 of the five conformational isomers. The initial ~ 100 -fs decay is due to the internal conversion between 1L_a and 1L_b states. The derived wobbling motion is also given in terms of the semiangle (θ). The long component represents the protein tumbling motion; see text.

of surrounding water molecules and possibly the associated (polar/charged) residues. The motions are induced by the sudden change of the tryptophan dipole moment. This local motion of water molecules has a similar time scale to the short residence time obtained in MD simulations^{36–38} for the equilibrium ground state. The MD simulations of residence time also gave an additional time scale,^{36–38} in tens of picoseconds, reflecting long-time dynamic exchange and equilibration in the ground state. When tryptophan is excited to the 1L_a state, the local equilibrium is shifted, and the system is in a nonequilibrium state. The observed long-time solvation dynamics reflects the temporal evolution from the initial nonequilibrium configuration to the

new equilibrium state around tryptophan in the excited state. During this process, dynamic exchange with bulk water always exists. The time scale to reach the new equilibrium is related to the residence time in the equilibrated excited state, which is probably similar to that found in MD simulations for the equilibrated ground state. Since the excited-state dipole ($\Delta\mu \approx 5$ D) is larger than that of the ground state, the dynamic evolution will finally result in an increase of water molecules around the tryptophan, as shown by our preliminary MD simulations.³⁹ The shorter the residence time, the faster the new equilibrium can be reached. Thus, the long-time component results from an integrated process with the system evolving from the nonequilibrium configuration to the new excited-state equilibrium, convoluted with dynamical exchange of the hydration water with bulk water. This slow dynamics, in fact, reflects a long-range translational motion.

B. Dynamic Quenching and Local Configuration. For all conformational isomers, we observed fluorescence quenching of tryptophan by neighboring protein residues. For example, at the red-side emission of 360 nm, we observed in the A form 37% quenching amplitude with a time constant of 29 ps, 18% with 35 ps in the B form, 10% with 51 ps in the N form, 10% with 100 ps in the F form, and 5% with 46 ps in the E form. From the basic to acidic conditions, the quenching components systematically decrease, reflecting more rigid local structures and/or increasing separation distances between W214 and the potential quencher(s). The observed wobbling motions in these isomers (Figure 9) disfavor the former and favor the latter. The quenching time constants from A to E isomers follow the trend of the derived two lifetimes; the faster the quenching, the shorter the other two lifetimes. Thus, the quenching component and multiple lifetime contributions do reflect a distribution of dynamic heterogeneous configurations of the W214 residue. The dynamic motion of W214 occurs on a time scale longer than several nanoseconds.

Bhagavan and co-workers²⁷ have recently reported a systematic examination of potential quenching residues around W214 in the N form using site-directed mutagenesis and identified R218 as the main quenching residue (Figure 1). They also observed that the mutation of R257, a residue at a distance of more than 11 Å away from W214, can eliminate the quenching by R218, indicating a local structural change induced by the mutation. The X-ray structure shows a distance of 3.81 Å between W214 and R218; both residues are in the same α -helix in domain IIA. At such a close distance it is possible that cation– π interactions between the two residues may result,^{40,41} leading to electron-transfer quenching, as suggested for other systems.⁴² The observed systematic decrease of the quenching contribution from A to E caused by R218 suggests a gradual loosening of contact between W214 and R218 in the same α -helix and a systematic local configuration change in domain IIA.

C. Hydration and Structural Flexibility of the N Conformation. At normal physiological conditions, the heart-shaped N form HSA adopts a globular structure with multiple binding sites.^{18,19} The common warfarin-binding site is located inside a 12-Å-deep crevice in domain IIA. W214 sits at the bottom of this water-filled binding pocket. Eight water molecules are shown in the X-ray structure within a distance of 7 Å (edge to edge) from the indole ring of W214, and three charged residues of K199, R218, and E450 are within 5 Å (Figure 1). Although W214 is deeply buried in the crevice, the highly polar environment, composed of trapped ordered water molecules and neighboring charged residues, leads to a considerable Stokes

shift of W214 with its emission peak at 338 nm, similar to that of a surface-type tryptophan.⁴³

In this deep binding site, we observed that W214 has the largest wobbling motion among all conformational isomers with a semiangle of 24°. Because the N-form HSA has the most tertiary structure content and W214 is buried inside the protein, the observed result is striking and indicates a *flexible* local protein structure, also consistent with the observation of dynamic quenching of W214 emission by R218. More important, we observed solvation dynamics around W214 in 133 ps (Table 2). Typically, deeply trapped water molecules in cavities or crevices have dynamic motions or residence times in the range from sub-nanoseconds to nanoseconds, as observed in other systems.^{7–9} As discussed above, this relatively long solvation component reflects the translational motion or residence time of the local hydration water in the binding pocket. The observed result is significant because of the intrinsic presence of water structure, although charged residue solvation may contribute due to the similar time scale of the wobbling motion of the tryptophan residue (174 ps). Thus, the binding pocket is “soft” in that the “trapped” water molecules are in fast dynamic exchange. The initial solvation component of 5 ps is also consistent with the local librational/rotational motions of trapped water molecules.

Both the observed solvation and the anisotropy dynamics reveal a highly flexible binding pocket. To assimilate and release various molecules in the circulatory system, the flexible structure is necessary for HSA to accommodate these ligands with different shapes and sizes. This conclusion is consistent with results revealed by X-ray structural studies that show considerable structural changes after ligand binding.^{12,13} The large plasticity for the carrier protein HSA ensures efficient transport of a variety of fatty acids, drugs, and small organic molecules in the blood through constant “breathing” motions to adopt binding recognition with fast-moving water acting as a lubricant.

D. Conformational Transition among Isomers. The stability, structure, and function of proteins are dependent on environmental pH values.⁴⁴ HSA undergoes a series of reversible conformational changes from acidic to basic conditions. At the neutral pH value of physiological conditions, the N isomer adopts a tertiary structure with all α -helices (Figure 1). From previous extensive studies,¹¹ especially using fluorescence and circular dichroism (CD) methods,^{45,46} it is shown that in the pH region of the N \rightarrow F transition (pH 5.0–3.5) the drastic structural change takes place primarily in domain III and domain II transforms to a molten-globule-like state, whereas domain I undergoes a structural rearrangement with minor changes in the secondary structure. Overall, a reduction of helical structure occurs in HSA whereas the content of sheet structure increases. In the acid-expansion region (pH < 3.5), a further noticeable reduction in the helix content takes place together with an increase in sheet structure, especially in domain I, resulting in a loss of interdomain and inter-subdomain contacts and a disruption of the structure in the hinge and linker regions. The albumin molecule is fully extended in the E form as its disulfide bonding structure allows. In the alkaline pH range between pH 7.4 and 9.0, the N \rightarrow B transition leads to a slight reduction in helical content and a small increase in sheet structure. The interdomains I and II experience a tertiary structural isomerization whereas domain III does not undergo structural alternation.

Under acidic conditions, the significant reduction of the tertiary structure and extension of the three interdomains disrupt the 12-Å crevice and destroy the local hydrophobic interactions

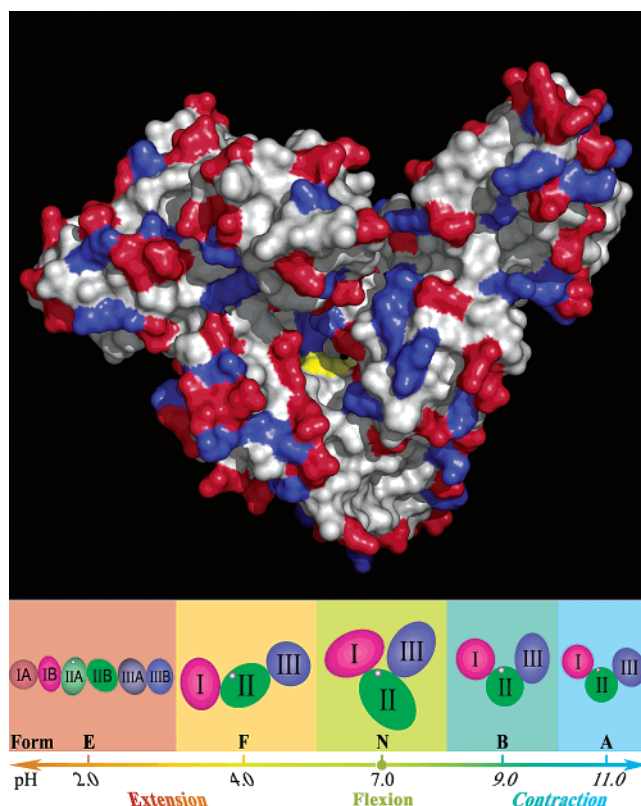


Figure 10. Top panel: Surface map of HSA with negative (red) and positive (blue) charge distributions. The crevice is shown in the center with tryptophan (yellow) sitting at its bottom. Bottom panel: Schematic representation of conformational transitions, from the contracted configuration in basic pH, to the flexible globule structure at neutral pH, and to the extended form in acidic pH. The location of W214 is indicated by the white dot in domain IIA.

between W214 and the residues from domain IIIA. Our observations of the fluorescence emission peak at about 330 nm and the more rigid local wobbling motions of about 13° in the F and E isomers suggest that W214 is confined in a hydrophobic environment with a partial exposure to water due to structural rearrangements. HSA is a highly charged protein with more than 180 charges at pH 7, for example, 36 aspartic acids, 62 glutamic acids, 59 lysines, and 24 arginines (Figure 10). The disruption of salt bridges or protonation of carboxyl groups (aspartic and glutamic acids) may lead to a significant charge distribution on the protein surface, resulting in a considerable water alignment in the hydration layer. The observed solvation dynamics in 100–200 ps is consistent with the highly ordered water molecules at lipid interfaces.^{31,47–49} When the solvation dynamics between E and F isomers (Figure 8) are compared, the faster water exchange in E is probably due to the wide protein extension with a reduced charge density at the protein surface. The initial fast decay component of 4–7 ps comes from the librational/rotational motions of these water clusters/networks. As discussed above, no ultrafast water motion in less than 1 ps was observed.

The N \rightarrow F conformational transition at a similar pH value has been found to be highly conserved among different species.¹¹ Such conservation has led to the belief that the F conformation occurs when the albumin molecule binds to the membrane surfaces of several tissues under physiological conditions at a lower pH value.¹⁶ The structural extension could be a necessary step for the albumin molecule to bind membrane surfaces to reach maximum contact area and then offload ligand(s) to the target. The observed time scale in 100–200 ps is ideal for

ordered water motions to match the interfacial water dynamics on membrane surfaces, which was observed recently to occur also in hundreds of picoseconds.^{31,49}

Under basic pH conditions, the tertiary and secondary structures suffer slight fluctuations. Surprisingly, we observed significant changes of solvation dynamics, and the water motion becomes much faster, occurring in 27–46 ps. The initial local water dynamics occurs in 1.6–2.3 ps. Both the solvation dynamics and the emission peak (~336 nm) reveal that W214 is located close to the protein surface, and thus the 10-Å crevice must open widely to allow more mobile water molecules into the IIA binding site. The similar emission peaks, but very different solvation dynamics, between N and B or A isomers result from the fact that the total Stokes shift is an integration of the local polarity while hydration dynamics reflect the rate of the local hydrogen bond making/breaking. For a similar polar environment, the trapped water in the crevice of the N form moves much slower than the mobile water at the protein surfaces in B and A isomers. The observed increase in quenching contribution reflects a more compact structure with a shorter separation between W214 and R218. Overall, these results indicate that in the B and A isomers the protein dynamically widens the crevice entrance and concurrently allows the globule structure to achieve more selective recognition.¹⁷

V. Conclusion

We reported here systematic studies of solvation dynamics and local rigidity in a series of reversible conformations of human serum albumin. The studies were made for the protein under different pH conditions, using the intrinsic tryptophan residue (W214) as the local optical probe, and the dynamics were probed with femtosecond time resolution. We observed a robust bimodal distribution of solvation time scales. For all conformational isomers, the initial solvation dynamics occurs in several picoseconds, reflecting local librational/rotational motions. As reported in our earlier studies,^{4–6,31} we can certainly resolve ultrafast solvation dynamics of tryptophan in bulk water in 200 fs, but we did not observe such initial ultrafast solvation dynamics for the proteins studied here. These findings contradict most MD simulations, and we suggest that the force fields used in simulations allow for large flexibility of the motion.

The observed second and longer-time solvation dynamics occurs in the range of tens to hundreds of picoseconds, depending on conformer, and reflects the exchange between the site-hydrated and bulk water; as pointed out above, the Stokes shift is an integration of solvation processes while solvation dynamics measure the rate of local hydrogen bond rearrangements. This long time scale depends on the local water structure in the crevice, known to be eight in number, and local chemical identity. The observed time scale is consistent with long residence times observed in MD simulations. However, in general, depending on local rigidity, polar/charged protein residues may contribute to the observed total solvation dynamics, but given the conformational and orientational correlations reported here, hydration by the smaller water molecules is major, as water molecules are already present in the crevice and will contribute solely or in association with residues to solvation. The result reported here for the shortening of this longer-time solvation, when HSA opens up its structure (conformer of basic pH), is consistent with the exchange being a major channel between crevice and bulk water.

Under the normal physiological conditions of neutral pH, the single W214 tryptophan in the binding site IIA is buried inside a 12-Å-deep crevice. Despite this closure, we observed fast

solvation dynamics of 133 ps, revealing a binding pocket capable of solvation on the fast time scale. Moreover, this globular native structure of the normal isomer shows the largest flexibility among all conformational isomers as revealed from measurement of the local wobbling motions of W214 tryptophan. The large plasticity of HSA is essential for the albumin molecule to accommodate a variety of ligands and to perform the transport function in the circulatory system. The observed time scale of ~100 ps is ideal for the trapped water molecules in the crevice at the binding site to maintain the local structural integrity as well as to maintain dynamic flexibility and lubrication in recognition and conformational transitions (Figure 10). The “lock-and-key or induced-fit” concept of molecular recognition is therefore incomplete without knowledge of dynamical solvation and plasticity of the protein.

Acknowledgment. This work was supported in part by the Petroleum Research Fund (PRF-42734-G4) and grants from the National Science Foundation to D.Z. (CHE-0517334) and A.Z. O.O. is grateful for a NASA Harriett Jenkins predoctoral fellowship. D.Z. thanks Professor Sherwin Singer for helpful discussions and Ya-Ting Kao for the initial help.

Supporting Information Available: All fitting parameters of amplitudes and time constants for transients in Figures 2–6 and the corresponding FRES. This material is available free of charge via the Internet at <http://pubs.acs.org>.

References and Notes

- Pal, S. K.; Zewail, A. H. *Chem. Rev.* **2004**, *104*, 2099. Pal, S. K.; Peon, J.; Bagchi, B.; Zewail, A. H. *J. Phys. Chem. B* **2002**, *106*, 12376.
- Mattos, C. *Trends Biochem. Sci.* **2002**, *27*, 203.
- Fenimore, P. W.; Frauenfelder, H.; McMahon, B. H.; Parak, F. G. *Proc. Natl. Acad. Sci. U.S.A.* **2002**, *99*, 16047. Frauenfelder, H.; Fenimore, P. W.; McMahon, B. H. *Biophys. Chem.* **2002**, *98*, 35.
- Zhong, D.; Pal, S. K.; Zhang, D.; Chan, S. I.; Zewail, A. H. *Proc. Natl. Acad. Sci. U.S.A.* **2002**, *99*, 13. Zhong, D.; Pal, S. K.; Zewail, A. H. *ChemPhysChem* **2001**, *2*, 219.
- Pal, S. K.; Peon, J.; Zewail, A. H. *Proc. Natl. Acad. Sci. U.S.A.* **2002**, *99*, 1763. Peon, J.; Pal, S. K.; Zewail, A. H. *Proc. Natl. Acad. Sci. U.S.A.* **2002**, *99*, 10964. Zhao, L.; Pal, S. K.; Xia, T.; Zewail, A. H. *Angew. Chem., Int. Ed.* **2004**, *43*, 60.
- Qiu, W.; Zhang, L.; Kao, Y.-T.; Lu, W.; Li, T.; Kim, J.; Sollenberger, G.; Wang, L.; Zhong, D. *J. Phys. Chem. B* **2005**, *109*, 16901.
- Kao, Y.-T.; Saxena, C.; Wang, L.; Sancar, A.; Zhong, D. *Proc. Natl. Acad. Sci. U.S.A.* **2005**, *102*, 16128.
- Jordanides, X. J.; Lang, M. J.; Song, X.; Fleming, G. R. *J. Phys. Chem. B* **1999**, *103*, 7995.
- Otting, G.; Liepinsh, E.; Wüthrich, K. *Science* **1991**, *254*, 974.
- Albumin Structure, Function and Uses*; Rosenoer, V. M., Oratz, M., Rothschild, M. A., Eds.; Pergamon: Oxford, U. K., 1977.
- Bertucci, C.; Domernici, E. *Curr. Med. Chem.* **2002**, *9*, 1463.
- Carter, D. C.; Ho, J. X. *Adv. Protein Chem.* **1994**, *45*, 153. He, X. M.; Carter, D. C. *Nature* **1992**, *358*, 209.
- Wardell, M.; Wang, Z.; Ho, J. X.; Robert, J.; Ruker, F.; Ruble, J.; Carter, D. C. *Biochem. Biophys. Res. Commun.* **2002**, *291*, 813.
- Luetscher, J. *J. Am. Chem. Soc.* **1939**, *61*, 2888.
- Forster, J. F. In *The Plasma Proteins*; Putman, F. W., Ed.; Academic Press: New York, 1960.
- Wilting, J.; Kremer, J. M. H.; Ijzerman, A. P.; Schulman, S. G. *Biochim. Biophys. Acta* **1982**, *706*, 96.
- Zurkowski, R. J.; Forster, J. F. *Biochemistry* **1974**, *13*, 3465.
- Curry, S.; Mandelkow, H.; Brick, P.; Franks, N. *Nat. Struct. Biol.* **1998**, *5*, 827.
- Zunszain, P. A.; Ghuman, J.; Komatsu, T.; Tsuchida, E.; Curry, S. *BMC Struct. Biol.* **2003**, *3*, 6.
- Benson, E. S.; Hallaway, B. E. *J. Biol. Chem.* **1970**, *245*, 4144.
- Kamal, J. K. A.; Zhao, L.; Zewail, A. H. *Proc. Natl. Acad. Sci. U.S.A.* **2004**, *101*, 13411.
- Sytnik, A.; Litvinyuk, I. *Proc. Natl. Acad. Sci. U.S.A.* **1996**, *93*, 12959.
- Flora, K.; Brennan, J. D.; Baker, G. A.; Doody, M. A.; Bright, F. V. *Biophys. J.* **1998**, *75*, 1084.
- Marzola, P.; Gratton, E. *J. Phys. Chem.* **1991**, *95*, 9488.
- Kamal, J. K. A.; Behere, D. V. *J. Biol. Inorg. Chem.* **2002**, *7*, 273.

- (26) Helms, M. K.; Petersen, C. E.; Bhagavan, N. V.; Jameson, D. M. *FEBS Lett.* **1997**, *408*, 67.
- (27) Siemiarczuk, A.; Petersen, C. E.; Ha, C.-E.; Yang, J.; Bhagavan, N. V. *Cell Biochem. Biophys.* **2004**, *41*, 1.
- (28) Zhong, D.; Douhal, A.; Zewail, A. H. *Proc. Natl. Acad. Sci. U.S.A.* **2000**, *97*, 14056.
- (29) Saxena, C.; Sancar, A.; Zhong, D. *J. Phys. Chem. B* **2004**, *108*, 18026.
- (30) Rava, R. P.; Spiro, T. G. *J. Phys. Chem.* **1985**, *89*, 1856.
- (31) Lu, W.; Kim, J.; Qiu, W.; Zhong, D. *Chem. Phys. Lett.* **2004**, *388*, 120.
- Lu, W.; Qiu, W.; Kim, J.; Okobiah, O.; Hu, J.; Gokel, G. W.; Zhong, D. *Chem. Phys. Lett.* **2004**, *394*, 415.
- (32) Shen, X. H.; Knutson, J. R. *J. Phys. Chem. B* **2001**, *105*, 6260.
- (33) Valeur, B.; Weber, G. *Photochem. Photobiol.* **1977**, *25*, 441.
- (34) Steiner, R. F. In *Topics in Fluorescence Spectroscopy*; Lakowicz, J. R., Ed.; Plenum Press: New York, 1991.
- (35) Nilsson, L.; Halle, B. *Proc. Natl. Acad. Sci. U.S.A.* **2005**, *102*, 13867.
- (36) Makarov, V. A.; Andrews, B. K.; Smith, P. E.; Pettitt, B. M. *Biophys. J.* **2000**, *79*, 2966.
- (37) Rocchi, C.; Bizzarri, A. R.; Cannistraro, S. *Phys. Rev. E* **1998**, *57*, 3315.
- (38) Luise, A.; Falconi, M.; Desideri, A. *Proteins* **2000**, *39*, 56.
- (39) Li, T.; Hassanali, A.; Zhong, D.; Singer, S., to be submitted for publication.
- (40) Dougherty, D. A. *Science* **1996**, *271*, 163.
- (41) Meyer, E. A.; Castellano, R. K.; Diederich, F. *Angew. Chem., Int. Ed.* **2003**, *42*, 1210.
- (42) Chen, Y.; Barkley, M. D. *Biochemistry* **1998**, *37*, 9976.
- (43) Lakowicz, J. R. *Principles of Fluorescence Spectroscopy*; Plenum Press: New York, 1999.
- (44) Matthew, J. B.; Gurd, F. R. N.; Garcia-Moreno, B.; March, K. L.; Shire, S. J. *Crit. Rev. Biochem.* **1985**, *18*, 91.
- (45) Dockal, M.; Carter, D. C.; Rüker, F. *J. Biol. Chem.* **2000**, *275*, 3042.
- (46) Kumar, Y.; Tayyab, S.; Muzammil, S. *Arch. Biochem. Biophys.* **2004**, *426*, 1.
- (47) Cheng, J.-X.; Pautot, S.; Weitz, D. A.; Xie, X. S. *Proc. Natl. Acad. Sci. U.S.A.* **2003**, *100*, 9826.
- (48) Faeder, J.; Ladanyi, B. M. *J. Phys. Chem. B* **2000**, *104*, 1033.
- (49) Willard, D. M.; Riter, R. E.; Levinger, N. E. *J. Am. Chem. Soc.* **1998**, *120*, 4151.